Materials Science & Engineering C 99 (2019) 853–862

Contents lists available at ScienceDirect

Materials Science & Engineering C

journal homepage: www.elsevier.com/locate/msec

Fabrication and characterization of biomimetic hydroxyapatite thin films for bone implants by direct ablation of a biogenic source

Gabriela Graziani[a], Matteo Berni[b,c], Alessandro Gambardella[a], Monica De Carolis[a], Maria Cristina Maltarello[d], Marco Boi[a], Gianluca Carnevale[e], Michele Bianchi[a,f,*]

[a] IRCCS Istituto Ortopedico Rizzoli, NanoBiotechnology Laboratory, Via di Barbiano 1/10, 40136 Bologna, Italy
[b] IRCCS Istituto Ortopedico Rizzoli, Laboratory of Biomechanics and Technology Innovation, Via di Barbiano 1/10, 40136 Bologna, Italy
[c] Department of Information Engineering, University of Brescia, Via Branze 38, 25123 Brescia, Italy
[d] IRCCS Istituto Ortopedico Rizzoli, Laboratory of Musculoskeletal Cell Biology, Via di Barbiano 1/10, 40136 Bologna, Italy
[e] Department of Surgery, Medicine, Dentistry and Morphological Sciences, University of Modena and Reggio Emilia, Via del Pozzo 71, 41124 Modena, Italy
[f] Center for Translational Neurophysiology of Speech and Communication, Fondazione Istituto Italiano di Tecnologia, Via Fossato di Mortara 17/19, Ferrara 44121, Italy

ARTICLE INFO

Keywords:
Calcium phosphates
Ion-substituted hydroxyapatite
Pulsed electron deposition
Nanostructured coatings
Bone regeneration
Orthopedics

ABSTRACT

Biomimetic bone apatite coatings were realized for the first time by the novel Ionized Jet Deposition technique. Bone coatings were deposited on titanium alloy substrates by pulsed electron ablation of deproteinized bovine bone shafts in order to resemble bone apatite as closely as possible. The composition, morphology and mechanical properties of the coatings were characterized by GI-XRD, FT-IR, SEM-EDS, AFM, contact angle measurements, micro-scratch and screw-insertion tests. Different post-treatment annealing conditions (from 350 °C to 425 °C) were investigated. Bone apatite coatings exhibited a nanostructured surface morphology and a composition closely resembling that of the deposition target (i.e. natural bone apatite), also regarding the presence of magnesium and sodium ions. Crystallinity and composition of the coatings were strongly influenced by annealing temperature and duration; in particular, upon annealing at 400 °C and above, a crystallinity similar to that of bone was achieved. Finally, adhesion to the titanium substrate and hydrophilicity were significantly enhanced upon annealing, all characteristics being known to have a strong positive impact on promoting host cells attachment, proliferation and differentiation.

1. Introduction

Calcium phosphates (CaP) coatings are commonly applied on the surface of bio-inert metallic bone implants and prosthetic devices to accelerate the formation of new bone and establish a firm bonding between the implant and the growing bone [1]. In particular, CaP thin films (thickness < 1 μm) are raising attention [2–4] compared to traditional, thick (> 30 μm), sprayed coatings due to a higher mechanical stability, lower tendency to cracking and delamination [5] and the possibility of obtaining a nanostructured surface texture able to boost platelet, protein and cell adhesion [6–8].

Aside from consolidated techniques for deposition of thin film deposition, such as Magnetron Sputtering (MS) and Pulsed Laser Deposition (PLD), Pulsed Electron Deposition (PED) is emerging as an effective and versatile method to fabricate nanostructured coatings. PED allows deposition on a wide variety of substrates, including heat-sensitive materials and a high fidelity in stoichiometry preservation from the deposition target to the coating [9–12]. PED setup is similar to that of the more widespread PLD: both techniques, in fact, rely on the ablation of a deposition target that is ionized as a plasma plume and accelerated toward the substrate, where it is deposited as a thin film [9]. Different from PLD, PED uses a pulsed electron beam as an ablation source, instead of laser source. As direct consequence of the different source (electrons vs. photons) PED presents some advantages, such as higher pulse energy, capability to ablate wide band-gap and highly reflective materials, and definitely lower costs for industrial scalability [13].

Among CaP coatings, biomimetic CaP coatings, that resemble the composition of natural bone apatite, can boost bone regeneration to a higher extent compared to stoichiometric HA or other CaP phases, by releasing in the surrounding environment all ions present in natural apatite in a suitable amount upon dissolution (i.e. i.e. Mg^{+}, CO_3^{2-}, Sr^{+}, K^{+}, etc.) [14,15]. In turn, suitable ion release can trigger stem cells homing and their osteogenic differentiation commitment, thus

* Corresponding author at: IRCCS Istituto Ortopedico Rizzoli, NanoBiotechnology Laboratory, Via di Barbiano 1/10, 40136 Bologna, Italy.
E-mail address: michele.bianchi@iit.it (M. Bianchi).

https://doi.org/10.1016/j.msec.2019.02.033
Received 19 June 2018; Received in revised form 11 January 2019; Accepted 10 February 2019
Available online 11 February 2019

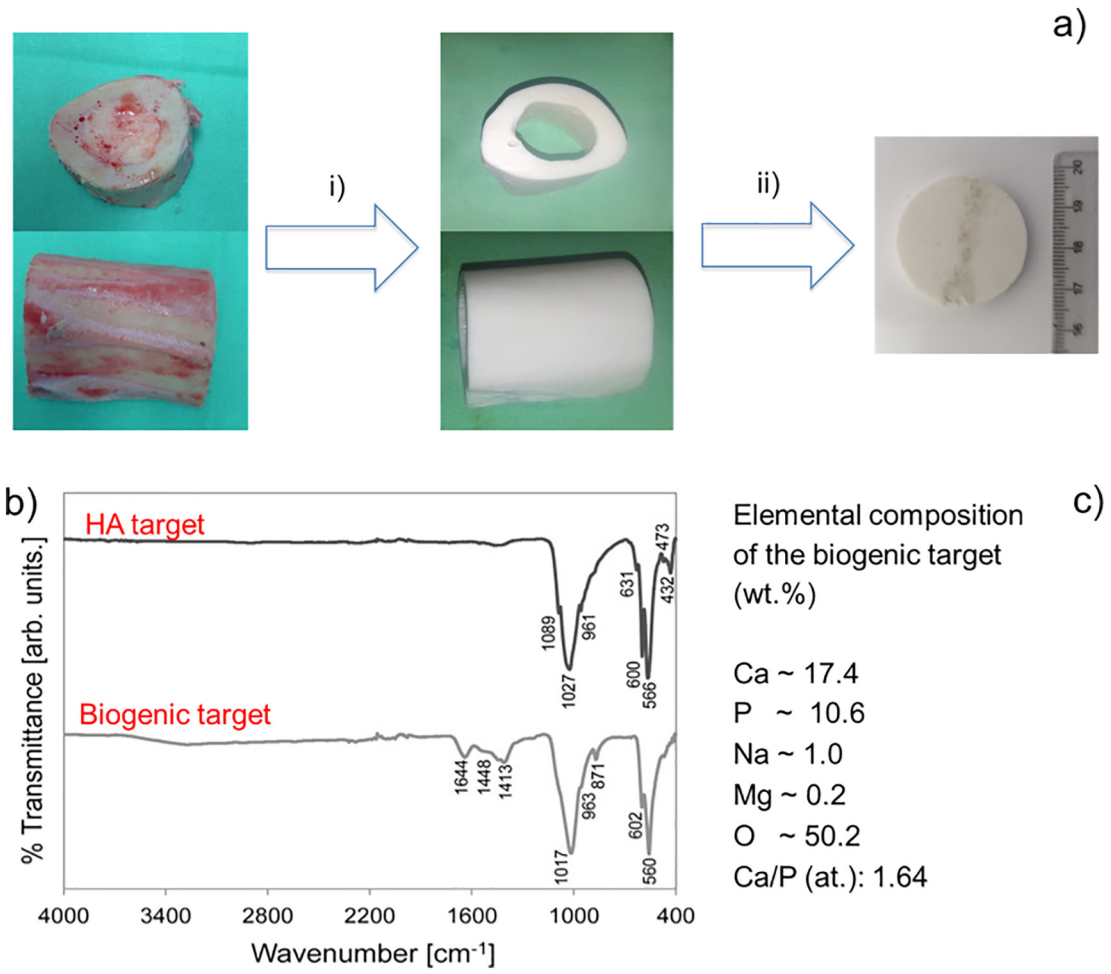

Fig. 1. Sketch of the fabrication of the biogenic target (a): bovine bone shafts before and after the deproteinization process (i) and after the machining step (ii) to achieve the final circular size. b) FTIR spectra of the deproteinized biogenic targets and of a stoichiometric HA target (b). c) Chemical composition by EDS of the biogenic target.

fastening the healing process and shortening the time required for achieving the optimum implant stability [16].

Recently, the Authors proved that biomimetic apatite films can be effectively obtained by direct ablation of a deproteinized biogenic source (i.e. a bone target) through the PED technique [17,18]. Composition and crystallinity very close to those of the bone target were achieved, upon post-treatment annealing [17]. Biomimetic apatite films also well-sustained host cells (human dental pulp stem cells, hDPSCs) proliferation and promoted their differentiation, even in absence of an osteogenic medium [18]. However, being the procedure of very recent introduction, several parameters need to be fully evaluated to optimize the coatings performance. In fact, a detailed characterization of film composition, micro-structural properties, morphology on the multiscale and mechanical characteristics, is needed, all being necessary parameters to identify the most promising candidates for further in vitro/in vivo evaluations. In this paper, the properties of biomimetic coatings deposited by PED directly from bone apatite sources will be investigated in terms of composition, surface morphology, crystallinity, hydrophilicity and adhesion to the substrate. The coatings will be deposited at room temperature, but different post-deposition annealing treatments will be investigated and compared, to optimize coatings crystallinity and physical-mechanical properties.

2. Materials and methods

2.1. Substrates

Medical grade titanium alloy disks (Grade 23 Titanium 6Al-4V ELI alloy, 5 mm of thickness, 5 or 20 mm of diameter, Citieffe S.r.l., Bologna, Italy) and silicon wafers (p-type doped monocrystalline (100) native silicon, size 10 × 10 mm, thickness 3 mm, Fondazione Bruno Kessler, Trento, Italy) were used after ultrasonic cleaning in isopropyl alcohol and water. No surface preparation in terms of polishing, machining, etching or surface patterning was carried out prior to deposition. Sterile titanium alloy dental screws (Grade 23 Titanium 6Al-4V ELI alloy, 1.6 mm × 8 mm, Auto-Drive Screw, Osteomed, USA) were used as received.

2.2. Preparation of the targets

Deposition targets were fabricated starting from bovine tibial cortical shafts, obtained from a local butcher at different times and from different animals. No further information about the animals (age, weight, etc.) was available at this stage; however they were not strictly necessary considered the scope of the present study. In fact, for the coatings to be exploitable, their efficacy must be negligent of the specific bone target selected. To this aim, different shafts were used to obtain the targets used in the study. Essentially no differences were noticed in the composition and morphology of the targets, or in those of

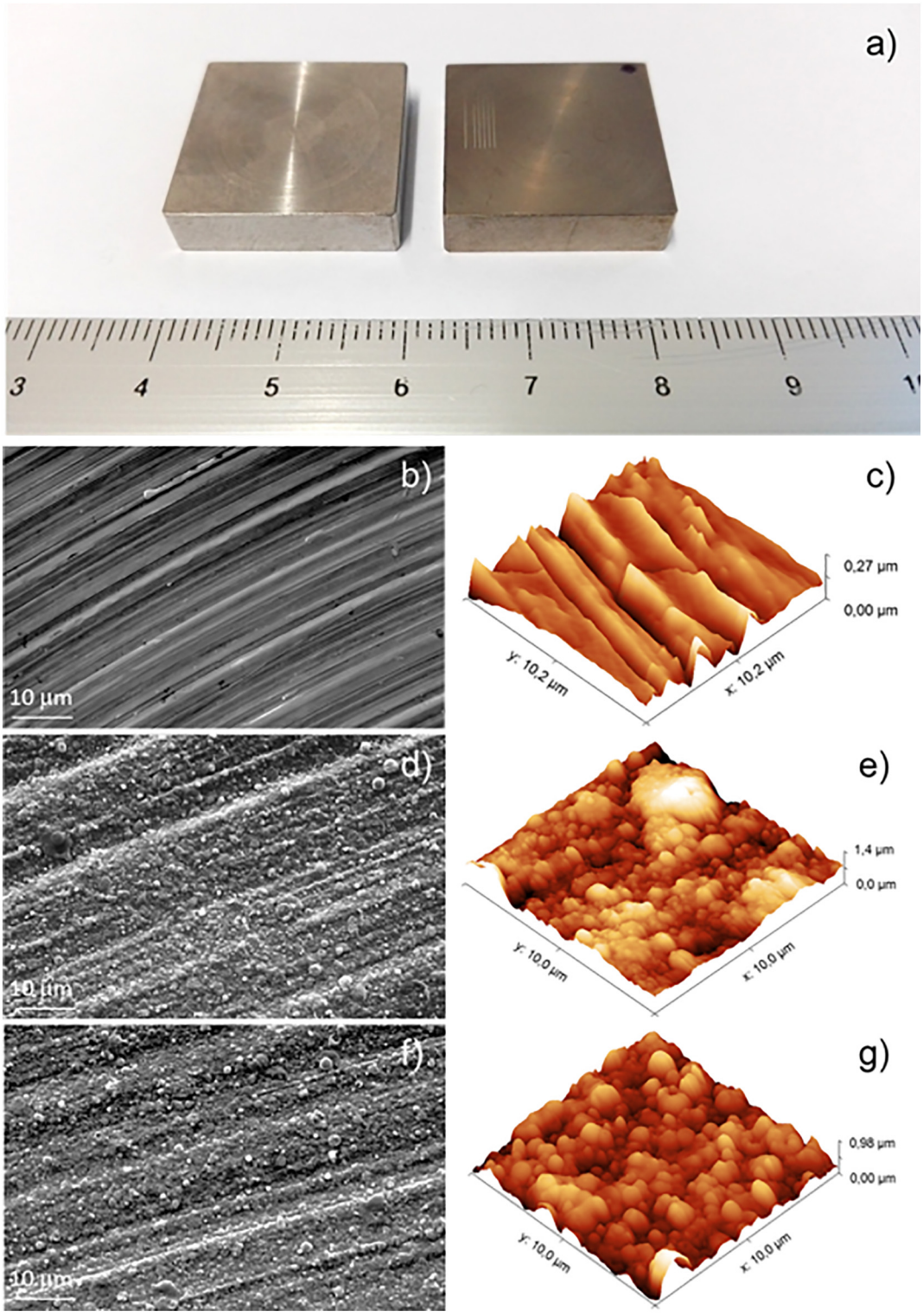

Fig. 2. Optical (a), SEM (b, d, f) and 3D AFM (c, e, g) images of the pristine titanium (a, left; b, c), Ti-ad (a, right; d, e) and Ti400-1 (f, g).

Table 1
Root mean square (RMS) values for the pristine titanium substrate for the biomimetic films as-deposited and heated according to different conditions.

Scan area (μm^2)	Ti	Ti_ad	Ti350-1	Ti375-1	Ti400-1	Ti425-1	Ti350-6	Ti375-6	Ti400-6	Ti425-6
50 × 50	265 ± 15	212 ± 27	331 ± 34	236 ± 40	328 ± 51	253 ± 15	235 ± 28	224 ± 22	310 ± 14	234 ± 18
10 × 10	200 ± 19	175 ± 19	257 ± 19	153 ± 8	234 ± 28	225 ± 13	226 ± 25	171 ± 16	251 ± 52	154 ± 9
2 × 2	33 ± 5	90 ± 25	167 ± 26	89 ± 26	111 ± 20	131 ± 30	115 ± 24	99 ± 10	130 ± 46	111 ± 25

Table 2
EDS elemental composition (wt% and at.% with standard deviation, s.d.) of Ti-ad and Ti400–1 films obtained.

	Ti-ad				Ti 400-1			
	wt%	s.d.	at. %	s.d.	wt%	s.d.	at. %	s.d.
Ca	18.02	0.03	11.16	0.01	14.7	0.5	9.3	0.3
P	7.59	0.03	6.07	0.01	6.3	0.3	5.2	0.2
Na	0.21	0.03	0.24	0.03	0.23	0.02	0.25	0.02
Mg	0.15	0.02	0.15	0.02	0.14	0.3	0.15	0.03
C	2.2	0.1	4.5	0.3	1.9	0.1	3.9	0.3
O	38.7	0.2	60.0	0.3	38.1	0.3	60.1	0.3
Ti	30.3	0.2	15.7	0.1	35.2	0.1	18.5	0.6
Al	1.79	0.01	1.64	0.01	2.00	0.07	1.86	0.08
V	1.09	0.02	0.53	0.01	1.41	0.04	0.70	0.02
Ca/P (at.)		1.84 ± 0.01				1.80 ± 0.12		

the coatings obtained from different targets. Bone shafts were firstly released of tendons, fat and bone marrow and then deproteinized by rinsing in the bleaching solution (daily refreshed) for 3 weeks until complete deproteinization. For deproteinization, bleaching solution containing 2.7 wt% of sodium hypochlorite was used without further purification. Deproteinization was verified by performing FT-IR after 7, 14 and 21 days bleaching and TGA at 21 days. Then, whitish apatite shafts were rinsed overnight in deionized water and ethanol to eliminate residual traces of the bleaching solution and left to dry at room temperature up to constant weight. Dry bone apatite shaft were cut and machined by a lathe into cylinders ($30 \times 5\,mm^2$) to have targets suitable for deposition by PED.

2.3. Thin film deposition

Thin films of biogenic apatite were realized by pulsed electron deposition in the novel Ionized Jet Deposition (IJD) setup (Noivion Srl, Rovereto, Italy) [19]. The deproteinized biogenic bone target was mounted on a rotating target holder and ablated by a fast pulse (100 ns) of high energy (10 J) and high-density ($109\,W\,cm^{-2}$) electrons. The "plasma plume" composed of the ablated material was directed toward a substrate mounted on a rotating holder and located at a distance of 10 cm from the target. The vacuum chamber was initially evacuated down to a base pressure of 1.0×10^{-7} mbar by a turbomolecular pump (EXT255H, Edwards, Crawley, England) and then raised by a controlled flow of oxygen (purity level = 99.999%) up to 3×10^{-4} mbar. The working voltage and the electron beam frequency were set at 17 kV and 7 Hz, respectively. The parameters used in this work have been selected based on preliminary studies regarding film growth at different acceleration voltages, frequencies and target-to-substrate distances. Films thickness of (450 ± 20 nm, corresponding to 30 min of deposition time), was also selected based on preliminary results [17].

2.4. Post deposition thermal treatments

After deposition, part of the films was annealed in air (LHT02/16 furnace, Nabertherm GmbH, Lilienthal, Germany) at different temperatures in the range 350 °C–425 °C. This range was selected based on two considerations: (i) an abrupt increase in crystallization of hydroxyapatite is expected around 400 °C, the exact temperature being dependent on the specific composition and the morphology of the hydroxyapatite layer [20] so heating in this range is expected to cause a transition from highly amorphous to partially crystalline coatings, (ii) higher temperatures can cause cracking phenomena, due to the onset of an extensive crystallization of the apatite (data not shown). The effect of heating duration was also taken into account that could also cause modifications in films crystallinity and composition. Films were hold at selected temperature for 1 or 6 h, with a heating/cooling ramp of $4\,°C\,min^{-1}$.

Based on the described consideration, 10 experimental groups were generated, labeled as in the following (Ti heating temperature [°C] - heating time [h]): Ti (uncoated titanium), Ti-ad (as deposited, i.e. not heat-treated), Ti 350-1, Ti350-6, Ti375-1, Ti375-6, Ti400-1, Ti400-6, Ti425-1, Ti425-6.

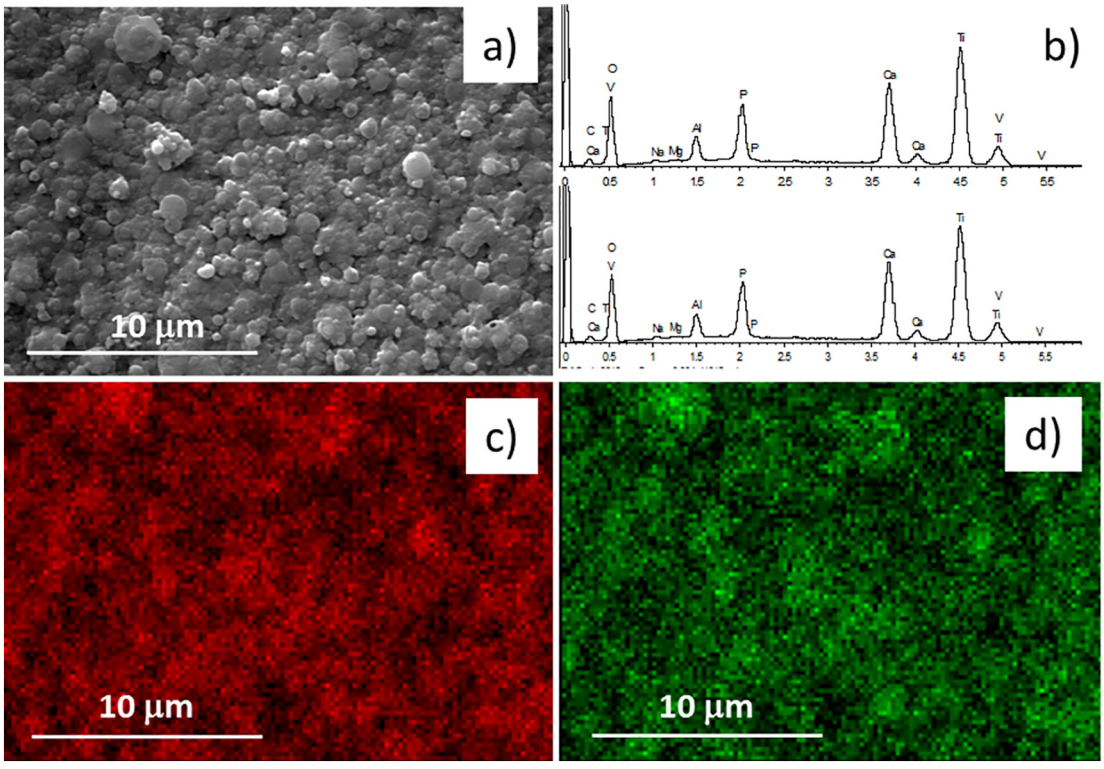

Fig. 3. SEM image of Ti-ad (a); representative EDS spectra (b; top: Ti-ad; bottom: Ti_400) and maps of Ca (c) and P distribution corresponding to a).

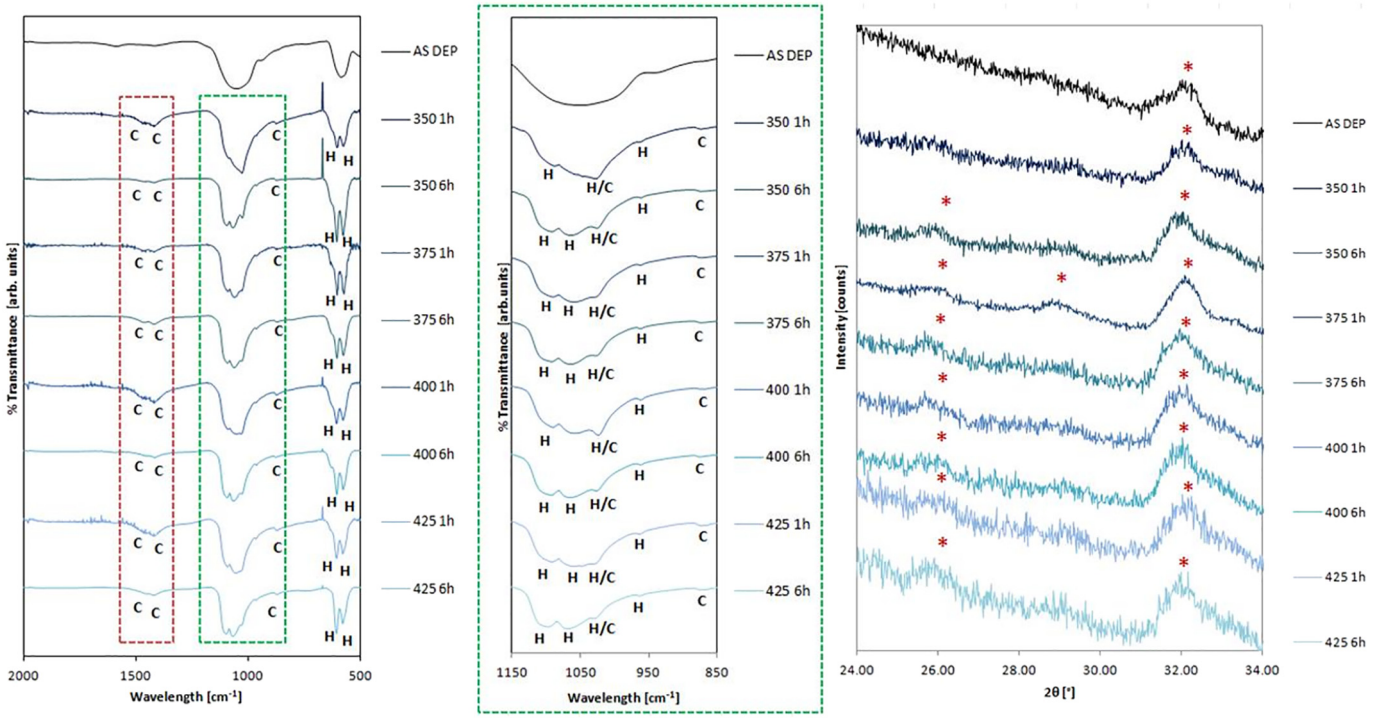

Fig. 4. (a) FT-IR spectra of the biomimetic films: bands characteristic of CHA (1455, 1419, 875 cm^{-1} [34,35] and HA (1090, 1030, 600, 570 cm^{-1} [36,37] are detected. (b) XRD patterns of the biomimetic films: all peaks detected are characteristic of hydroxyapatite and/or CHA. A sure discrimination between CHA and HA is not possible here, as low crystallinity causes XRD peaks to be broad and ill-defined.

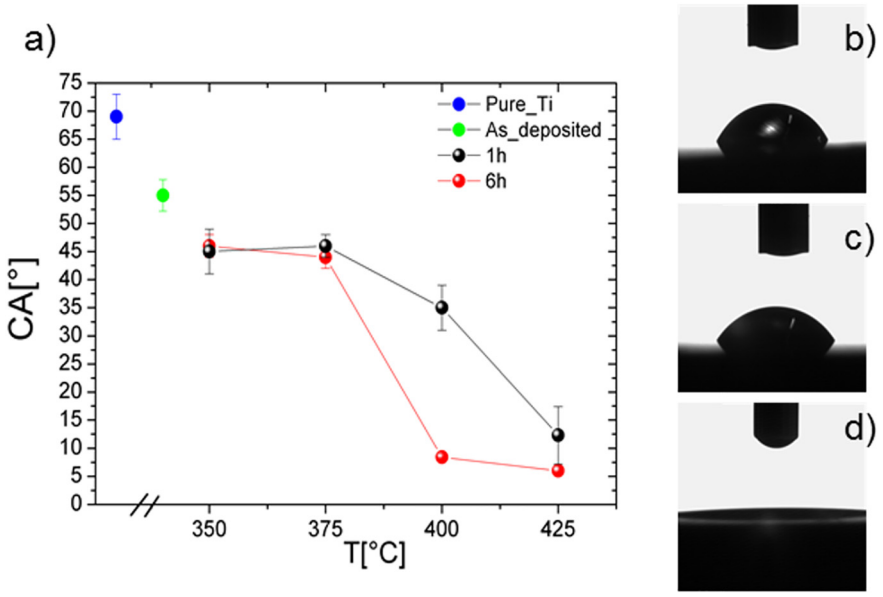

Fig. 5. Plot reporting the values of water contact angle (CA) for pristine Ti and biomimetic films (a); optical images of the water drop on Ti (b), Ti-ad (c) and Ti-425-1 (d).

2.5. Film characterization

Film thickness, topography and roughness were evaluated by an Atomic Force Microscope (AFM) operating in semi-contact mode at ambient conditions (Stand-Alone SMENA AFM, NT-MDT, Moscow, Russia). For the evaluation of film thickness, depositions were carried out on flat silicon substrates, as high surface roughness of titanium substrate hinders a correct evaluation of this parameter. To guarantee that the very same conditions are achieved (i.e. same target-substrate distance as for titanium substrates and that the same amount of ablated material that reaches the substrate), silicon wafers were put inside the deposition chamber together with the titanium disks on suitable stands. The AFM was equipped with a SFC050 head, mounting silicon probes with a guaranteed curvature radius of about 10 nm and resonance frequencies of 190–330 kHz (NSG series probes, NT-MDT, Moscow, RU). The reported values for the Root Mean Square roughness (RMS) were calculated as average of the values obtained upon several non-overlapping sample regions, whose dimensions ranged from (10 × 10) μm^2 to (2 × 2) μm^2. All the images were unfiltered, except for a 2nd order leveling, and acquired with a resolution of (512 × 512) pixels.

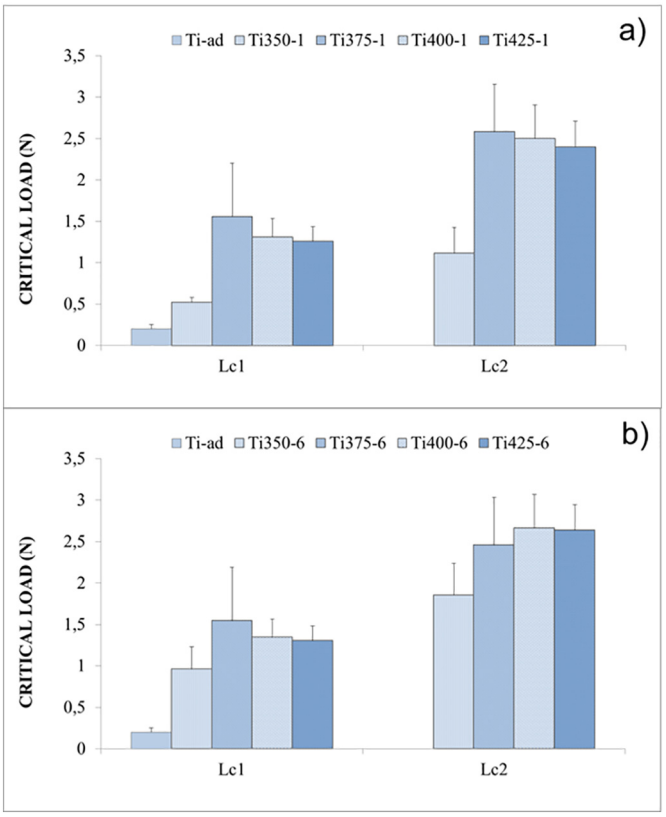

Fig. 6. Results of micro-scratch tests. Critical failure loads for partial (Lc1) and complete (Lc2) delamination for as-deposited and heated samples for 1 h (a) and 6 (h).

Coating morphology was analyzed by a Scanning Electron Microscope (EVO/MA10, ZEISS) equipped with an Energy Dispersive X-ray Spectrometry system (EDS, INCA Energy 200, Oxford Instruments, Abingdon-on-Thames, UK) for the elemental composition. Spot chemical analyses and elemental maps (1500 s) were acquired at both working at 20 kV. Special attention was devoted to the presence of trace ions in the coatings (mostly, Mg and Na).

Film composition was analyzed by GI-XRD (Panalytical X'Pert PRO, grazing incidence mode, angle $\omega = 2^{\circ}$, $\varphi = 180^{\circ}$, scan step size 0.0167, time per step 250.190). XRD patterns were collected in a range $2\theta = 3–15^{\circ}$ and $20–34^{\circ}$ to investigate the areas relevant for calcium phosphates while excluding the peaks of titanium. Functional groups in the coatings were examined by FT-IR (Perkin Elmer Spectrum two, resolution 1 cm^{-1}, accumulations 64 scans), to determine calcium phosphate phases composing the films.

Surface wettability was characterized by water contact angle (CA) measurement (Digidrop contact angle meter, GBX Instrumentation Scientifique, Romance, France). The volume of the drop was ~0.50 μL, corresponding to a contact radius with the surface, uncoated or coated, of ~0.5 mm. Contact angle values were acquired on at least five different positions over the sample surface and the mean value was provided.

To evaluate the adhesion of the films to titanium substrates, micro-scratch tests were performed following the procedures reported in the relative standard normative [21], by using a Micro-Scratch Tester (MST, CSM Instruments — Anton Paar S.r.l, Peseux, Switzerland). Specifically, a conical Rockwell C stylus with spherical apex indenter tip (angle 120° and sphere radius 100 μm) subjected to a progressive normal loading from 0.01 to 10 N moved across the surface of the coated sample with an indenter traverse speed of 10 mm min^{-1} and a loading rate of 10 N min^{-1}. For each considered group, two coated-titanium substrates were investigated on the surface of which six scratches were made. The worn tracks were investigated to determine the failure modes of the coating and associate them with the critical normal load at which they occurred (Lcn).

Additional qualitative information about the degree of adhesion of the films under conditions closer to the real ones, were provided by inserting and removing auto-drive titanium dental screws coated with biomimetic films in a rigid polyurethane foam simulating cortical bone (Sawbone®, Washington, USA). Briefly, biomimetic coatings were deposited on one side of the titanium dental screws; then the deposition was repeated by rotating the screw of 180°, in order to cover the whole screw surface. Part of the samples were annealed according to the conditions determined in the first stages of the research (400 °C, 1 h); as deposited screws were examined for comparison sake to confirm the positive effects of the thermal treatment on coatings adhesion. Coated screws were inserted then removed from a Sawbone block (mimicking the mechanical properties of cortical bone) at a fixed torque load. Then, eventual damage caused to the coatings was evaluated by examining the surface of the screws by SEM, before and after insertion/removal procedure. Five as-deposited coated screws and five annealed coated screws were tested, and compared to uncoated references.

2.6. Statistics

All data are presented as mean ± standard deviation. For the analysis of the results of micro-scratch tests, after assessment of the normality of data distribution by the Kolmogorov–Smirnov test, the Kruskal-Wallis test was used to compare critical load values among different samples. If a significant difference was observed, comparison was than performed between each coupling by using two-sided Wilcoxon rank sum test with a level of statistical significance $\alpha = 0.05$.

3. Results and discussion

3.1. Target preparation and characterization

The process used for obtaining the biogenic bone targets is schematically depicted in Fig. 1a. After 3 weeks of immersion in the sodium hypochlorite solution, deproteinized bone shafts appeared whitish and the relative FT-IR spectra did not show clear bands owing to amide I and II of collagen (1659 and 1555 cm^{-1}, Fig. 1b), indicating the effectiveness of the deproteinization process. Bone target showed bands characteristic of functional groups of carbonated HA (CHA) - 1448, 1413 cm^{-1}, (asymmetrical and symmetrical stretching modes of ν_3 CO_3), 1017 cm^{-1} (antisymmetric stretching mode v_3PO_4), 871 cm^{-1}(ν_2 CO_3) - and, to a lower extent, octacalcium phosphate (OCP) - 1644 cm^{-1} (ν_2 H_2O bend), 963 cm^{-1} (ν_1 PO_4 symmetric stretch) - and hydroxyapatite (HA) - 963 cm^{-1} (ν_1 PO_4 symmetric stretch), 602 and 566 cm^{-1} (ν_4 PO_4 antisymmetric bend), 469 cm^{-1} (ν_2PO_4 bend). Stoichiometric HA target, exhibiting all characteristic bands of HA: 1089 and 1027 cm^{-1} (ν_3 PO_4 antisymmetric stretch), 961 cm^{-1} (ν_1 PO_4 symmetric stretch), 631 cm^{-1} (ν_LOH or H_2O libration), 600 and 566 cm^{-1} (ν_4 PO_4 antisymmetric bend), 473 cm^{-1} (ν_2 PO_4 bend) [22–25], has been reported for clarity sake. EDS analysis of the bone target confirmed the presence of Na and Mg among the other elements (Fig. 1c), in comparable amounts to what can be found in literature relating to bovine bone composition [26].

3.2. Biomimetic apatite films deposited on titanium alloy substrates

SEM and AFM images of biomimetic films (thickness ~ 450 nm) deposited on titanium alloy substrate are in Fig. 2. Morphology and grain size did not significantly vary between as-deposited and heat-treated samples and among samples treated at different annealing conditions (data not shown), thus, only SEM and AFM images of Ti400-1 are reported in Fig. 2, for brevity sake.

Films obtained on the rough titanium substrates are highly

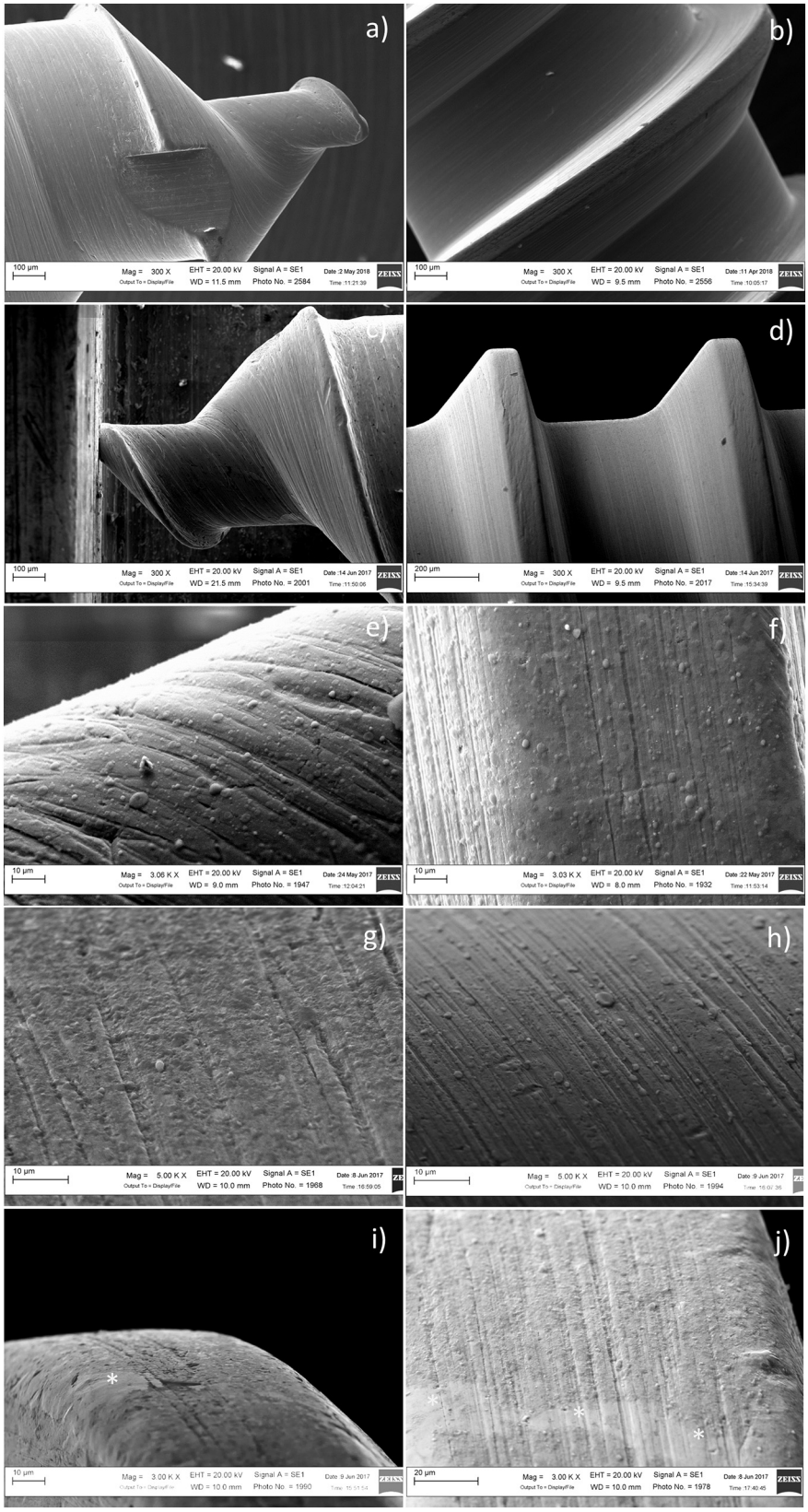

Fig. 7. Results of the insertion test. Representative SEM images of a dental screws before (a, b) and after coating deposition (c–d). Details of a coated screw with untreated (e) and 400 °C treated (f) biomimetic coating before insertion in Sawbone block. Details of a coated screw with an untreated (g, i) and 400 °C treated (h, j) biomimetic coatings after removal from Sawbone block.

homogenous (Fig. 2c, e) and composed by round-shaped grains (Fig. 2d, f), characteristic of the techniques based on pulsed electron or laser ablation [27,28], with mean lateral size ranging from ~50 nm to ~200 nm. Machining features and surface roughness at the micro-scale are generally selected by the implants producers to maximize implant primary stability and promote integration in the surrounding bone [29,30]. Thus, it is desired that a coating does not modify those feature (micro-topography), while, at the same time, providing additional functional properties to the implant. Further, the nanostructured coating, by directly reflecting into a higher surface area, is envisaged to promote both in vitro and in vivo protein adhesion and thus bone cell adhesion and proliferation and eventually new bone formation [31,32].

As evidenced by the SEM images, the film deposition has only slightly modified the original micro structure of the substrate as its machining traces, a few hundreds of nanometers high and separated by a distance ranging from fraction of microns to a few microns (Fig. 2b), were simply mimicked and thus are still clearly detectable (Fig. 2d-f); in other words, the deposition is conformal. In a previous work, this group has suggested that the above "memory" effect, which is characteristic of the deposition of thin films on high aspect-ratio substrates, takes place over a range of thicknesses that can be assessed quantitatively by statistical methods [33]. In the present case, the multiscale arrangement between the micro-rough substrate and the nanostructured coating can be also appreciated by observing the RMS values extracted by the corresponding AFM images, and reported in Table 1. The images evidence how the size of the corrugation of the bare substrate affects strongly the film morphology at 50×50 and $10 \times 10\,\mu m^2$ while at $2 \times 2\,\mu m^2$ – e.g. at length scales comparable with the intra-scratches spacings – the film is no longer conformal; this is reflected by the dramatic alteration of the corresponding RMS values with respect to the uncoated surface. Finally, no significant variation was evidenced in the RMS with different temperatures and/or heating times.

3.3. Coating composition and phase structure

The results of the compositional analysis have been reported in Table 2. Due to substantial chemical similarity among all the samples, representative results for Ti-ad and Ti 400-1 have been reported. Noticeably, trace ions characteristics of ionic substitution in bone apatite are preserved in the deposited films, including Mg and Na, similarly to what observed in the starting bone target (Fig. 1c). This demonstrated the IJD technique allows obtaining a perfect correspondence between the composition of the target material and that of the obtained coatings, also for what regards trace ions.

As can be inferred from Fig. 3c and d, the distribution of the elements was highly homogenous across the whole samples.

FT-IR and XRD (Fig. 4) indicate that the coatings are constituted by hydroxyapatite (HA) and carbonated hydroxyapatite (CHA), as the following bands are detected: 1455, 1419 cm^{-1}, (asymmetrical and symmetrical stretching modes of $CO_3\nu_3$), 871 cm^{-1}(ν_2 CO_3), 1089 and 1030 cm^{-1} (ν_3 PO_4 antisymmetric stretch), 600 and 570 cm^{-1} (ν_4 PO_4 antisymmetric bend) [22]. The presence of octacalcium phosphate (OCP) can be excluded as no peaks are detected in the 2ϑ = 3–15° area of XRD patterns, for any of the samples (data not shown).

No significant differences are assessed in the composition of the coatings by any of the techniques, as no phases other than HA and CHA are detected, independently of heating temperature and duration. All samples heated for 6 h, however, present a lower content of CHA (see bands at 1465, 1429, and 870 cm^{-1}) with respect to those heated for only 1 h.

Interestingly, the similarity of the coatings to real bone is denoted by the presence of a band at 870 cm^{-1} in FT-IR spectra, that according to Ref. [38], is characteristic of carbonates, but also characterizes calcium-deficient and/or non-stoichiometric HA.

Together with composition, also crystallinity plays a key role in determining the behavior of the cells, as it determines the speed and intensity of ion-release. In particular, a crystallinity similar to that of bone, is desired. Films deposited by PED at room temperature are amorphous or scarcely crystalline, as can be noted by the broad shape of FT-IR bands and XRD peaks, which would make them experience too fast a dissolution and leads to coating detachment, causing scarce adhesion and proliferation of host cells [18]. As a consequence, post-treatment annealing was needed. Crystallinity degree is significantly lower for samples AD and 350-1h, while it is essentially identical for the others. It must be noted here, that slight variations in crystallinity depending on the heating temperature, could be concealed by the wide shape of XRD peaks, characteristic of grazing incidence setup.

Preliminary data indicate that a crystallinity similar to that of bone as the one deposited by IJD, significantly increases adhesion of the films and promotes host cells behavior [17,18]. However, the temperature needed to obtain a suitable crystallinity can significantly vary, depending on apatite composition and on the heating environment [20].

3.4. Film hydrophilicity

The apposition of the thin apatite layer increased the wettability of the surface compared to the uncoated titanium substrate, that is moderately hydrophobic (≈68°, see Fig. 5). Thermal treatments above 400 °C significantly increased the wettability of the samples, up to nearly superhydrophilic values (5 ÷ 15°) for samples treated at 425 °C.

Among the range of chemo-physical stimuli contributing to determine the final wettability of the implant, surface chemistry, surface energy and micro-, sub-micro- and nanoscale topographical features play a major role [39]. Thus, as already observed in previous studies regarding natural or synthetic hydroxyapatite deposited by IJD [9,17,40], here surface chemistry overwhelmed the surface roughness (that was similar among the different samples) into determine the final wettability of the material. Most studies have demonstrated that hydrophilic surfaces are capable of enhancing cells adhesion, proliferation, differentiation and bone mineralization compared to hydrophobic surfaces [41,42]. As a consequence, biological properties of heated samples are expected to be significantly improved compared to as-deposited CaP.

3.5. Adhesion to flat titanium

Critical failure loads for partial (Lc1) and complete (Lc2) delamination have been reported in Fig. 6.

As-deposited films exhibited scarce adhesion to the titanium substrate; however, the relatively low-temperature annealing process significantly increased the resistance of the coatings to both partial and complete delamination. Films Ti-350-1h show a slight increase in the adhesion, that becomes more significant when heating time is prolonged to 6 h. All films heated at 400 °C and above exhibit similar adhesion, significantly higher than that of as-deposited and Ti-350-1h films. No obvious effect of the annealing time on the adhesion was detected, apart from samples treated at 350 °C, where the longer annealing time increased the resistance to both partial and complete delamination. Failure loads for partial and complete delamination were in good agreement with results for HA coatings deposited by competitive techniques, being mainly PLD [43,44], reporting critical load up to ~2–3 N for films with similar properties. The results of the scratch tests closely match data obtained by FT-IR and XRD concerning films crystallinity, that is very scarce for as-deposited films, slightly increases for Ti-350-1h and is remarkably higher for the other heating conditions. Films annealed at 350 °C, for which a difference in crystallinity exists depending on heating duration (that is not assessed for any other heating condition), are the only ones to exhibit relevant differences in adhesion. This clearly indicates that adhesion is essentially determined by film crystallinity.

Based on the data obtained, heating at 400 °C for 1 h was selected as the most promising annealing condition, based on the following

considerations: (i) As-deposited films and films annealed at 350 °C exhibited too low an adhesion to the substrate, good adhesion being one of the key parameters to determine the performance of coatings, hence they were discarded. (ii) The decrease in the content of CHA with respect to HA observed in samples heated for 6 h compared to 1 h, instead, pushed to exclude the first, as it decreases the similarity to the deposition target. This similarity, in fact, is expected to boost biological behavior of the coatings, based on the biomimetic principle. (iii) Hydrophilicity of the films increases at 400 °C and above, which is another desired characteristic that favors host cells adhesion. (iv) No differences are assessed between Ti-400-1h and Ti-425-1h, so heating at the lowest temperature is preferred, as cracking phenomena were already observed at 500 °C (data not shown) and slight variations in the propensity to cracking could be experienced for varying coatings characteristics.

3.6. Dental screw insertion test

An important task of an industrially-scalable deposition technique is the possibility to coat non-prototypical surfaces, i.e. objects having complex shape in the 3D space and relatively important lateral dimension. To test this ability with our IJD system and to better evaluate the adhesion degree of the biomimetic films under conditions resembling more closely the real ones (i.e. simulating the insertion of a dental screw in cortical bone). To this aim auto-drive titanium dental screws were coated with biomimetic films in a two-step procedure, as described in the “Materials and Methods” section.

SEM images of coated screws indicated that coating obtained are highly homogeneous, both on the top of the ridges as well as inside the screw valleys, as no uncoated areas were spotted in any part of the screws surface (Fig. 7c-f). Moreover, the original micro-structure of the screw surface, as its machining lines, was preserved after the film deposition as expected by the results of deposition on machined titanium seen before.

Importantly, inspection of the screw surface after (insertion and) removal from the Sawbone blocks indicated that most of the coating has not been damaged by the operation (Fig. 7g, h), besides some small portions located at the ridges which have been detached in correspondence to the higher mechanical stress to which they were subjected (Fig. 7i, j). Finally, no evident effect of the thermal treatment on the adhesion of the film to the titanium substrate was detected under the investigated conditions, indicating that the deposition of highly rough surfaces can promote coating adhesion, even in the least favorable conditions.

Overall, the results of the insertion test suggested an adhesion degree of the biomimetic films to the titanium screws suitable for real applications.

4. Conclusions

In this work, the morphological, chemical, micro-structural and mechanical characteristics of biomimetic thin films for bone regeneration have been reported and compared. Biomimetic coatings were manufactured by pulsed electron ablation of a biogenic target. Different thermal treatments have been compared (from 350 °C to 425 °C, 1 h and 6 h of treatment) to optimize coatings crystallinity and adhesion to the substrate.

Based on the obtained results, the following conclusion can be derived:

* Biomimetic coatings can be effectively manufactured by direct ablation of a fully-deproteinized biogenic source. EDS analysis revealed that the coatings exhibit composition well mimicking that of the target, particularly with regard to Ca/P ratio (≈1.8 for the bone target; ≈1.6 for the bone coating) and amount of Mg and Na ions, and a nanostructured surface texture providing high surface roughness, especially at small length scales (RMS of bare Ti ≈ 30 nm; RMS of coated Ti from 90 to 170 nm, see Table 1).
* As deposited coatings are highly amorphous, hence post deposition treatments are recommended to enhance coatings characteristics. Upon annealing, crystallinity of the coatings can be optimized, so as to resemble that of bone (Fig. 4). As a consequence of annealing, hydrophilicity (water contact angle of 55° for as-deposited coating; ≈5°–10° for annealed coatings) and adhesion to the substrate (Fig. 6) also increase, both being key parameters to guarantee pro-osseointegrative efficacy.
* For the specific conditions (i.e. target material, nanostructured surface texture, sub-micrometric thickness), a significant transition in crystallinity from highly amorphous to partially crystalline apatite is achieved at temperatures of 350 °C and above, also depending on heating duration.
* The selected post-deposition treatment consists in heating the coated materials at 400 °C for 1 h. For these coatings, remarkable adhesion is found also for deposition onto objects of complex shape, such as dental screws, with minimal removal of coating after insertion/removal of the coated screw from the Sawbone blocks.

In view of these conclusions we believe that the coatings are very promising for application to bone implants. An extensive characterization is in progress to fully investigate in vitro behavior of the developed coatings, also depending on deposition and post-deposition conditions.

Acknowledgements

The research was partially funded by INAIL INAIL-Istituto Nazionale Assicurazione Infortuni sul Lavoro (National Institute for Insurance against Accidents at Work), Project METACOS “Trattamento delle amputazioni mediante osteointegrazione” and “5 × 1000 2015”, provided by Rizzoli Orthopedic Institute. The Authors would like to acknowledge Mr. Carmelo Carcasio for technical assistance for the fabrication of the biogenic targets.

References

[1] A.W.G. Jinhua's, S.C.G. Leeuwenburgh, J.A. Jansen, Wet-chemical deposition of functional coatings for bone implantology, Macromol. Biosci. 10 (2010) 1316–1329.
[2] J.V. Rau, I. Antoniac, M. Filipescu, C. Cotrut, M. Fosca, L.C. Nistor, R. Birjega, M. Dinescu, Hydroxyapatite coatings on mg-ca alloy prepared by pulsed laser deposition: properties and corrosion resistance in simulated body fluid, Ceram. Int. 44 (2018) 16678–16687.
[3] K.A. Prosolov, K.S. Popova, O.A. Belyavskaya, J.V. Rau, K.A. Gross, A. Ubelis, Yu.P. Sharkeev, RF magnetron-sputtered coatings deposited from biphasic calcium phosphate targets for biomedical implant applications, Bioact Mater 2 (2017) 170–176.
[4] M. Curcio, A. De Bonis, M. Fosca, A. Santagata, R. Teghil, J.V. Rau, Pulsed laser-deposited composite carbon–glass–ceramic films with improved hardness, J. Mater. Sci. 52 (2017) 9140.
[5] X. Zhao, S. Ng, B.C. Heng, J. Guo, L. Ma, T.T. Tan, K.W. Ng, S.C. Loo, Cytotoxicity of hydroxyapatite nanoparticles is shape and cell dependent, Arch. Toxicol. 87 (2013) 1037–1052.
[6] J.Y. Park, C.H. Gemmell, J.E. Davies, Platelet interactions with titanium: modulation of platelet activity by surface topography, Biomaterials 22 (2001) 2671–2682.
[7] A. Klymov, L. Prodanov, E. Lamers, J.A. Jansen, X.F. Walboomers, Understanding the role of nano-topography on the surface of a bone-implant, Biomater. Sci. 1 (2013) 135–151.
[8] I.V. Smirnov, J.V. Rau, M. Fosca, A. De Bonis, A. Latini, R. Teghil, V.I. Kalita, A.Yu. Fedotov, S.V. Gudkov, A.E. Baranchikov, V.S. Komlev, Structural modification of titanium surface by octacalcium phosphate via pulsed laser deposition and chemical treatment, Bioact Mater 2 (2017) 101–107.
[9] M. Bianchi, L. Degli Esposti, A. Ballardini, F. Liscio, M. Berni, A. Gambardella, S.C.G. Leeuwenburgh, S. Sprio, A. Tampieri, M. Iafisco, Strontium doped calcium phosphate coatings on poly (etheretherketone) (PEEK) by pulsed electron deposition, Surf. Coat. Technol. 319 (2017) 191–199.
[10] M. Bianchi, A. Gambardella, M. Berni, S. Panseri, M. Montesi, N. Lopomo, A. Tampieri, M. Marcacci, A. Russo, Surface morphology, tribological properties and in vitro biocompatibility of nanostructured zirconia thin films, J. Mater. Sci. Mater. Med. 27 (2017) 1–10.
[11] M. Berni, N. Lopomo, G. Marchiori, A. Gambardella, M. Boi, M. Bianchi, A. Visani,

P. Pavan, A. Russo, M. Marcacci, Tribological characterization of zirconia coatings deposited on Ti6Al4V components for orthopedic applications, Mater. Sci. Eng. C 62 (2016) 643–655.
[12] D. Bellucci, M. Bianchi, G. Graziani, A. Gambardella, M. Berni, A. Russo, V. Cannillo, Pulsed Electron deposition of nanostructured bioactive glass coatings for biomedical applications, Ceram. Int. 43 (2017) 15862–15867.
[13] J.E. Mathis, H.M. Christen, Factors that influence particle formation during pulsed electron deposition of YBCO precursors, Phys. C 459 (2007) 47–51.
[14] G. Graziani, M. Bianchi, E. Sassoni, A. Russo, M. Marcacci, Ion-substituted calcium phosphate coatings deposited by plasma-assisted techniques: a review, Mater. Sci. Eng. C 74 (2017) 219–229.
[15] J.V. Rau, I. Cacciotti, S. Laureti, M. Fosca, G. Varvaro, A. Latini, Bioactive, nanostructured Si-substituted hydroxyapatite coatings on titanium prepared by pulsed laser deposition, J Biomed Mater Res B Appl Biomater 103 (2015) 1621–1631.
[16] A. Hoppe, N.S. Güldal, A.R. Boccaccini, A review of the biological response to ionic dissolution products from bioactive glasses and glass-ceramics, Biomaterials 32 (2011) 2757–2774.
[17] M. Bianchi, A. Gambardella, G. Graziani, F. Liscio, M.C. Maltarello, M. Boi, M. Berni, D. Bellucci, G. Marchiori, F. Valle, A. Russo, M. Marcacci, Plasma-assisted deposition of bone apatite-like thin films from natural apatite, Mater. Lett. 199 (2017) 32–36.
[18] M. Bianchi, A. Pisciotta, L. Bertoni, M. Berni, A. Gambardella, A. Visani, A. Russo, A. de Pol, G. Carnevale, Osteogenic differentiation of hDPSCs on biogenic bone apatite thin films, Stem Cells Int. 2017 (2017) 3579283.
[19] WO 2013/186697 A2, L. Skocdopolova, NOIVION S.r.l., inventor, WO Patent 2013/186697, (2013 Dec 25), p. A2.
[20] Y. Yanga, K. Kim, J.L. Ong, A review on calcium phosphate coatings produced using a sputtering process—an alternative to plasma spraying, Biomaterials 26 (2005) 327–337.
[21] International Organization for Standardization, Fine ceramics (Advanced Ceramics, Advanced Technical Ceramics) — Determination of Adhesion of Ceramic Coatings by Scratch Testing, (2016) (ISO standard no. 20502).
[22] J. Tao, Chapter twenty-two - FTIR and Raman studies of structure and bonding in mineral and organic–mineral composites, Methods Enzymol. 532 (2013) 533–556.
[23] I. Rehman, W. Bonfield, Characterization of hydroxyapatite and carbonated apatite by photo acoustic FTIR spectroscopy, J. Mater. Sci. Mater. Med. 8 (1) (1997).
[24] A. Antonakos, E. Liarokapis, T. Leventouri, Micro-Raman and FTIR studies of synthetic and natural apatites, Biomaterials 28 (2007) 3043–3054.
[25] L. Berzina-Cimdina, N. Borodajenko, Prof. Theophanides Theophile (Ed.), Research of Calcium Phosphates Using Fourier Transform Infrared Spectroscopy - Materials Science, Engineering and Technology, 2012 ISBN: 978-953-51-0537-4, (InTech).
[26] S.V. Dorozhkin, M. Epple, Biological and medical significance of calcium phosphates, Angew. Chem. Int. Ed. 41 (2002) 3130–3146.
[27] L. Floroian, B. Savu, G. Stanciu, A.C. Popescu, F. Sima, I.N. Mihailescu, R. Mustata, L.E. Sima, S.M. Petrescu, D. Tanaskovic, D. Janackovic, Nanostructured bioglass thin films synthesized by pulsed laser deposition: CSLM, FTIR investigations and in vitro, Biotests Appl. Surf. Sci. 255 (2008) 3056–3062.
[28] D.G. Wang, C.Z. Chen, Q.S. Ma, Q.P. Jin, H.C. Li, A study on in vitro and in vivo bioactivity of HA/45S5 composite films by pulsed laser deposition, Appl. Surf. Sci. 270 (2013) 667–674.
[29] W.R. Lacefield, Materials characteristics of uncoated/ceramic-coated implant materials, Adv. Dent. Res. 13 (2007) 21–26.
[30] Z. Simon, P.A. Watson, Biomimetic dental implants – new ways to enhance Osseointegration, J. Can. Dent. Assoc. 68 (2002) 286–288.
[31] R.A. Gittens, R. Olivares-Navarrete, T. McLachlan, Y. Cai, S.L. Hyzy, J.M. Schneider, Z. Schwartz, K.H. Sandhage, B.D. Boyan, Differential responses of osteoblast lineage cells to nanotopographically-modified, microroughened titanium–aluminum–vanadium alloy surfaces, Biomaterials 33 (2012) 8986–8994.
[32] A. Klymov, L. Prodanov, E. Lamers, J.A. Jansen, X.F. Walboomers, Understanding the role of nano-topography on the surface of a bone-implant, Biomater. Sci. 1 (2013) 135–151.
[33] A. Gambardella, M. Berni, A. Russo, M. Bianchi, A comparative study of the growth dynamics of zirconia thin films deposited by ionized jet deposition onto different substrates, Surf. Coat. Technol. 337 (2018) 306–312.
[34] I. Rehman, W. Bonfield, Characterization of hydroxyapatite and carbonated apatite by photo acoustic FTIR spectroscopy, J. Mater. Sci. Mater. Med. 8 (1997) 1–4.
[35] A. Antonakos, E. Liarokapis, T. Leventouri, Micro-Raman and FTIR studies of synthetic and natural apatites, Biomaterials 28 (2007) 3043–3054.
[36] J. Tao, FTIR and Raman studies of structure and bonding in mineral and organic–mineral composites, Methods Enzymol. 532 (2013) 533–556.
[37] S. Koutsopoulos, Synthesis and characterization of hydroxyapatite crystals: a review study on the analytical methods, J. Biomed. Mater. Res. 62 (2002) 600–612.
[38] L. Berzina-Cimdina, N. Borodajenko, Research of calcium phosphates using Fourier transform infrared spectroscopy, infrared spectroscopy, Materials Science, Engineering and Technology, Chapter 6, 2012, pp. 123–148.
[39] R. Junker, A. Dimakis, M. Thoneick, J.A. Jansen, Effects of implant surface coatings and composition on bone integration: a systematic review, Clin. Oral Implants Res. 20 (2009) 185–206.
[40] M. Boi, M. Bianchi, A. Gambardella, F. Liscio, S. Kaciulis, A. Visani, M. Barbalinardo, F. Valle, M. Iafisco, L. Lungaro, S. Milita, M. Cavallini, M. Marcacci, A. Russo, Tough and adhesive nanostructured calcium phosphate thin films deposited by the pulsed plasma deposition method, RSC Adv. 5 (2015) 78561–78571.
[41] C. Eriksson, H. Nygren, K. Ohlson, Implantation of hydrophilic and hydrophobic titanium discs in rat tibia: cellular reactions on the surfaces during the first 3 weeks in bone, Biomaterials 25 (2004) 759–766.
[42] M.M. Bornstein, P. Valderrama, A.A. Jones, T.G. Wilson, R. Seibl, D.L. Cochran, Bone apposition around two different sandblasted and acid-etched titanium implant surfaces: a histomorphometric study in canine mandibles, Clin. Oral Implants Res. 19 (2008) 233–241.
[43] J.M. Fernández-Pradas, M.V. García-Cuenca, L. Clèries, G. Sardin, J.L. Morenza, Influence of the interface layer on the adhesion of pulsed laser deposited hydroxyapatite coatings on titanium alloy, Appl. Surf. Sci. 195 (2002) 31–37.
[44] S. Johnson, M. Haluska, R.J. Narayan, R.L. Snyder, In situ annealing of hydroxyapatite thin films, Mater. Sci. Eng. C 26 (2006) 1312–1316.